Testing the APLC on the LAO ExAO testbed

Sandrine J. Thomas [a], Rémi Soummer [b], Daren Dillon [a], Bruce Macintosh [a, c], Julia W Evans [c], Donald Gavel [a], Anand Sivaramakrishnan [b], Christian Marois [d], Ben R. Oppenheimer [b]

[a] Laboratory for Adaptive Optics, UCSC, 1156 High Street, Santa Cruz, CA, USA;
[b] Astrophysics, American Museum of Natural History, 79th street at Central Park West, New York, NY 10024;
[c] Lawrence Livermore National Laboratory, 7000 East Ave, Livermore 94550 , CA, USA ;
[d] Herzberg Institute of Astrophysics, 5071 West Saanich Road, Victoria , BC V9E 2E7, Canada.

ABSTRACT

We present testbed results of the Apodized Pupil Lyot Coronagraph (APLC) at the Laboratory for Adaptive Optics (LAO). This coronagraph is being built for the Gemini Planet Imager (GPI). The apodizer component is manufactured with a halftone technique using black chrome microdots on glass. Testing this APLC (like any other coronagraph) requires extremely good wavefront correction, which is obtained to the 1nm RMS level on the Extreme Adaptive Optics (ExAO) visible testbed of the Laboratory Adaptive optics (LAO) at the University of Santa Cruz. With this testbed, we investigated the performance of the APLC coronagraph and more particularly the effect of the apodizer profile accuracy on the contrast. We obtained the first image of a dark zone in a coronagraphic image with a MEMS deformable mirror. Finally, we compare the resulting contrast to predictions made with a wavefront propagation model of the testbed to understand the effects of phase and amplitude errors on the final contrast.

Keywords: Extreme adaptive optics, High contrast imaging

1. INTRODUCTION

During the last decade, astronomers have detected about 300 planets around stars via different indirect techniques such as spectroscopy or transits. However, those techniques only give us the existence of a planet without additional information. Direct imaging combined with spectroscopy of the discovered planet will allow us to determine its composition. This increasing interest in the direct observations of planet around stars pushes adaptive optics techniques to its extreme. The goal is to achieve contrast as high as 10^{-7} from the ground or 10^{-9} from space. Our current systems are limited by the dynamic range of the CCD as well as the diffraction rings of the PSF close to the central peak. Moreover, aberrations of the system and the atmosphere turbulence add speckles in the region of interest, reducing further the dynamic range. The use of a coronagraph combined with a very good correction of the wavefront will eliminate most of the light coming from the parent star and allow detection of Jupiter mass planets. This is the goal that many groups are attempting to achieve, both for ground-based systems, such as Gemini Planet Imager (GPI)[1] and SPHERE,[2,3] and space based systems such as the Terrestrial Planet Finder (TPF). Both ground-based imagers hope to achieve contrast of between 10^{-6} and 10^{-7} in order to image young Jupiter-like planets while TPF has more stringent contrast requirements for imaging earth-like planets. Testbed experiments in support of TPF are on-going on the High Contrast Imaging Testbed (HCIT).[4]

Our work on the ExAO testbed in the Laboratory for Adaptive Optics (LAO) at University of California Santa Cruz supports the Gemini Planet Imager (GPI).[5] This testbed allows us to test key components of GPI such as Micro-electrical-mechanical-systems (MEMS) deformable mirror, rarely used in astronomy and the coronagraph. The choice of the coronagraph used in GPI and tested here is the APLC which is a variant from the classical Lyot

Further author information: (Send correspondence to S.J. Thomas.)
S.J.Thomas: E-mail: sthomas@ucolick.org, Telephone: 1 831 459 3870

Adaptive Optics Systems, edited by Norbert Hubin, Claire E. Max, Peter L. Wizinowich,
Proc. of SPIE Vol. 7015, 70156I, (2008)
0277-786X/08/$18 · doi: 10.1117/12.789691

Coronagraph for which the pupil edges are smoothed out by an apodized pupil. Optimal apodization functions are given by prolate spheroidal functions.[6] Previous results have been obtained with the same testbed using a prolate shaped pupil and a focal plane mask.[7] The prolate shaped pupil scatters the light in a privileged direction blocked down stream by the appropriate focal plane mask. While these masks give reasonable results of the order of 5.10^7 at $5\lambda/d$, the APLC gives improved results.

Section 2 briefly explains the APLC principle. Section 3 gives some details on the manufacture of the APLC and tests on the LAO testbed. Section 4 and section 5 give results of the tests with and without wavefront correction. Finally we show some results from the astrometric and photometric grid in section 6.

2. APLC THEORY

The Apodized Lyot Coronagraph is an improved version of the Lyot Coronagraph designed to achieve better contrasts. In this section we are summarizing the principle of the APLC. The reader can find more explanations in Aime et al. and Soummer et al.[6,8] Fig. 1 gives the principle of the APLC layout.

Figure 1. APLC basic formalism.

The only difference from the classical coronagraph is the presence of the apodizer in the pupil before the focal plane mask. Following the notation given in the literature, $P(r)$ is the wavefront amplitude at the pupil plane and $\Phi(r)$ the transmission of the apodizer. The amplitude at the upstream pupil is therefore:

$$\Psi(r) = P(r)\Phi(r) \tag{1}$$

The next step is to put a mask in the focal plane. The mask has a transmission of 0 inside the coronagraphic mask and 1 outside. At the Lyot stop plane, the wavefront is then:

$$\Psi_C(r) = P(r)\Phi(r) - \frac{\epsilon}{\lambda^2 f^2}\int_P \Phi(u)\widehat{M}\left(\frac{r-u}{\lambda f}\right)du, \tag{2}$$

where $\widehat{\ }$ is the Fourier Transform. This general relation is valid for any arbitrary aperture shape (rectangular, circular or elliptical, with or without central obstruction and secondary mirror supports), and any mask shape, Soummer (2005). In this equation we assume that the focal lengths of the successive optical systems are identical (if not, an appropriate change of variables leads to the same result). We re-orientate the axis in the opposite direction and omit the -1 proportionality factor for better readability. The formal problem is to find the mask $M(r)$ and the apodizer $\Phi(r)$ that provide the best cancellation possible inside the Lyot stop, identical to the entrance pupil in this case.

The above partition of the wavefront (eq. 2) gives a physical understanding of coronagraphy as a destructive interference between the pupil wave $\Psi(r)$ and the wave diffracted by the mask (the convolution integral). The APLC solution is to smooth out the pupil transmission so that the wave diffracted by the mask matches the pupil wave. The total extinction ($\Psi_C(r)$=0) is obtained if the wave diffracted by the mask (the convolution integral) is

equal to the initial pupil amplitude. In more mathematical terms, this means that $\Phi(r)$ must be the eigenfunction of the convolution integral in 2. The solution is the pupil apodization which produces the most concentrated star light behind a given focal plane mask (and thus blocked). This formal problem has been solved analytically for rectangular and circular unobstructed apertures,,[6,8] involving linear and circular prolate functions.[9,10] In the general case, formal solutions exist[11,12] and are the eigenfunction of the 2-D integral equation:

$$\int_P \Phi(u)\widehat{M}\,(r-u)\,du = \Lambda\Phi(r) \tag{3}$$

The solution $\Phi(r)$ corresponds to the largest eigenvalue Λ_0 , and to the maximum encircled energy behind the focal plane mask. The mask size is directly related to the eigenvalue, and therefore, for a given mask size, a unique apodization function exists. The expression of the residual wavefront inside the Lyot stop for circular and rectangular geometries is the same for the general case:

$$\Psi_C^+(r) = \Psi_A(r)(1-\epsilon\Lambda_0) \tag{4}$$

(the $^+$ signies this is just after the Lyot stop). As detailed in previous work the wavefront is therefore simply proportional to the initial apodization function, with a constant of proportionality (1-$\epsilon\Lambda_0$).

3. DIRECT TESTS OF THE APLC

3.1 Manufacture of the apodizers

The apodizers and the focal plane mask are manufactured with a halftone technique using black chrome microdots on glass by Jenoptik *. The apodizer transmission is obtained by randomly distributing 2μm square dots over the glass. Fig. 2 shows views of the apodizer with successive magnification. In the following tests, we will only present the case of a simple apodizer without central obstruction.

Figure 2. Image of the apodizers at successive magnification. The left image shows the full apodizer with central obstruction and astrometric grid. The grid on this apodizer is used as an astrometric and photometric reference for the planet discovery. We give more results on the use of this grid in section 6.

Fig. 3 gives the dimensions of the apodizer used for this experiment. The pupil size is 10mm and the FPM size is 350 μm. The FPM was manufactured by a black chrome disk deposit on glass. Finally we used a metal Lyot stop of diameter 4.03 mm.

3.2 The tesbed

As mentioned in the introduction, we used the Extreme AO testbed located at the laboratory for Adaptive Optics (LAO) in Santa Cruz to test the concept of the APLC (Fig. 4). This testbed uses a reduced number of optical elements to decrease the sources of wavefront errors and is equipped with a high-precision interferometer (PSDI for Phase Shifting Diffraction Interferometer[13]) as wavefront sensor. Coronagraphy requires extremely

*www.jenotik.com

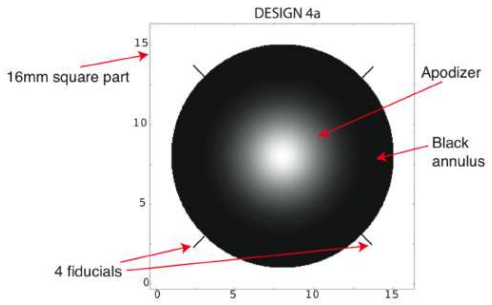

Figure 3. Dimension of the apodizer.

good wavefront quality in order to concentrate the light in the core of the PSF. We also want to eliminate all unwanted speckles coming either from the atmospherical turbulence or the aberrations in the system. The wavefront correction is made using MEMS technology. More specifically, the device has 32×32 actuators. By comparison, the final instrument will have 64×64 actuators and is under testing at the LAO. With this testbed, we were able to achieve wavefront corrections of less than 1 nm RMS over controllable spatial frequencies. Fig. 4 gives the layout of the testbed but a more detailed description can be found in a paper by Evans et al.[14] The APLC is composed of three main components each placed in three different planes: the entrance pupil before the MEMS is used for the apodizer, the FPM (CI on the figure) is put in the first focal plane and the LS is put at the conjugate of the pupil plane in between the two spherical mirrors. This location is called Lyot plane. The first set of tests has been done with a good gold flat mirror ($\lambda/100$ surface quality) to quantify the quality of the apodizer and allow easier comparison between simulations and experiments. It also allowed us to define the alignment procedure. However, there are some additional aberrations introduced by the other optics in the system. Because we need the best wavefront possible, wavefront correction is obtained at lower spatial frequencies using the MEMS deformable mirror.

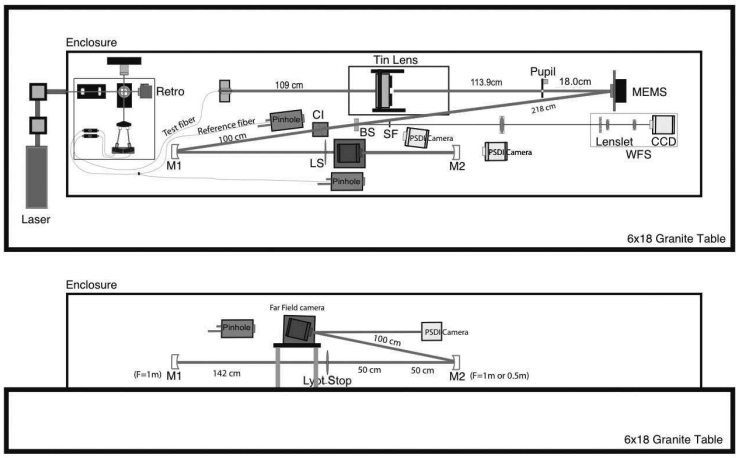

Figure 4. Testbed layout. The important planes are the pupil (apodizer), CI (Focal plane mask) and LS (Lyot Stop).

The apodizer itself does not introduce much aberrations. Here are the wavefront maps taken with the PSDI. PSDI measurements give a wavefront error of 1.6nm RMS with the apodizer and 1.2nm RMS without. The difference in quadrature is less than 1nm (cf. Fig. 5).

For all these experiments, we had the option to image those planes of interest, pupil imaging mode or farfield imaging mode, by replacing only one element in the system (mirror M2, Fig. 4). This feature turned out to be very useful to help aligning the different component of the APLC. Images acquired at those positions can be

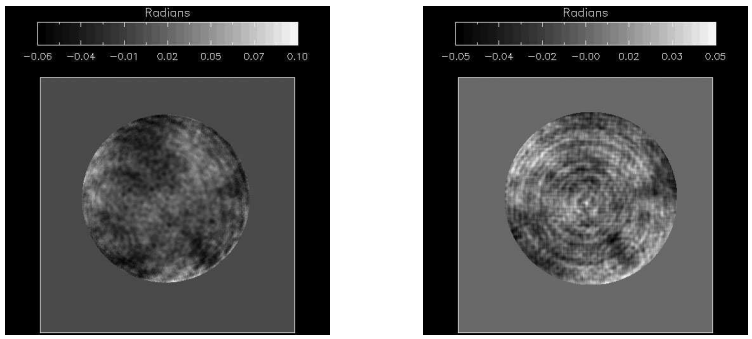

Figure 5. Wavefront maps taken with PSDI. The phase is in radians. Left is without the APLC and right is with APLC.

easily compared with models of the expected intensity using a Fresnel propagation simulator. The final contrast is finally calculated from the image.

4. TEST OF THE APLC WITHOUT WAVEFRONT CORRECTION

4.1 Results with the flats

As mentioned above, we first tested the APLC using the high quality flat mirror i.e without wavefront correction. However, as mentioned previously the optics in the system are of very good quality making possible to get very good performance of the coronagraph. In this section, we show the successive planes of the systems to demonstrate the good behavior of the APLC. We first imaged the apodizer alone, using the pupil imaging mode, to get its profile. Fig. 6 shows an image of the pupil with the apodizer as well as its radial average profile.

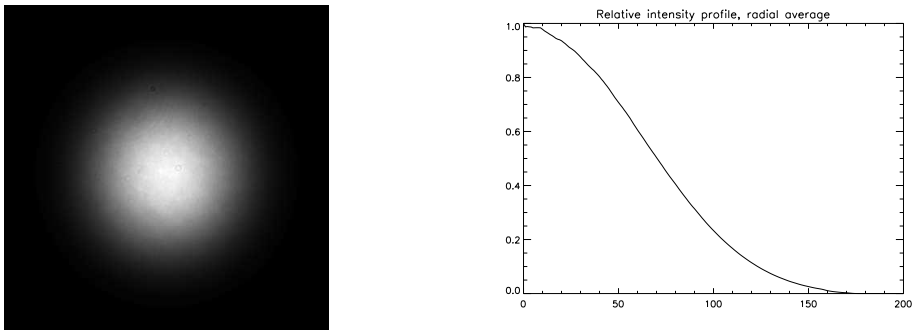

Figure 6. Left: Image of the apodizer. Right: radial average of the apodizers.

In Fig. 7 we show a comparison between the apodizer measured profile and the theoretical profile. Both profiles are in very good agreement with a maximum absolute error of 3% in transmission at about half the radius. This implies that the microdots might have some effects on the wavefront, some can be attributed to the actual shape of the dots and resonant effects (because the wavelength is comparable to the dot size). These errors will have to be calibrated for the final apodizer. The maximum relative error on the transmission is 20% at the edge of the pupil. Because of the very low transmission at the edge of the apodizer, there is a slight uncertainty in the determination of the apodizer diameter from the data. We considered the effect of a possible error on the diameter and show the results in Fig. 8 , using a scaling factor for the apodizer diameter. In this case the agreement is excellent with a maximum absolute error of 0.6%, and a maximum relative error on the transmission is 2.5% close to the edge of the apodizer. This result suggests that the observed error in Fig. 7 may be due in part to an error on the experimental determination of the diameter. We will investigate further the actual cause of the apodizer transmission precision in a future paper.

When we put the FPM in the system, the results are a good match to the theory. The intensity in the pupil plane is expected to be proportional to the apodizer inside the pupil and to show a large scale bright ringing

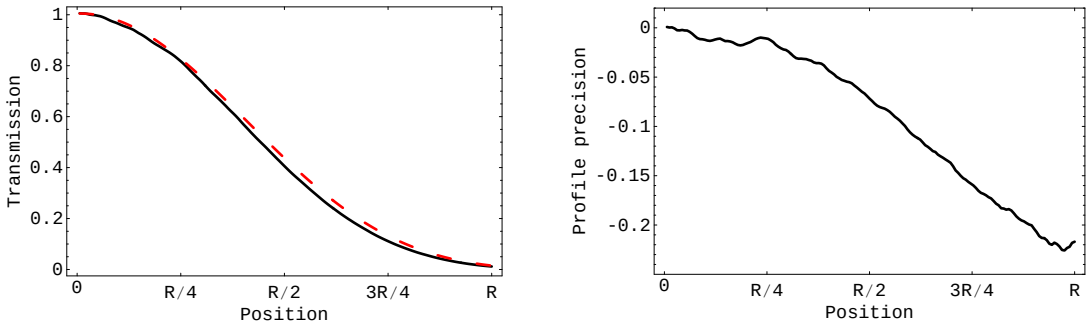

Figure 7. Left panel: comparison between the apodizer profile (black) measured with the testbed and the theoretical apodizer profile (red). The relative precision between the two profiles is shown in the right panel (20% relative error at the edge of the profile).

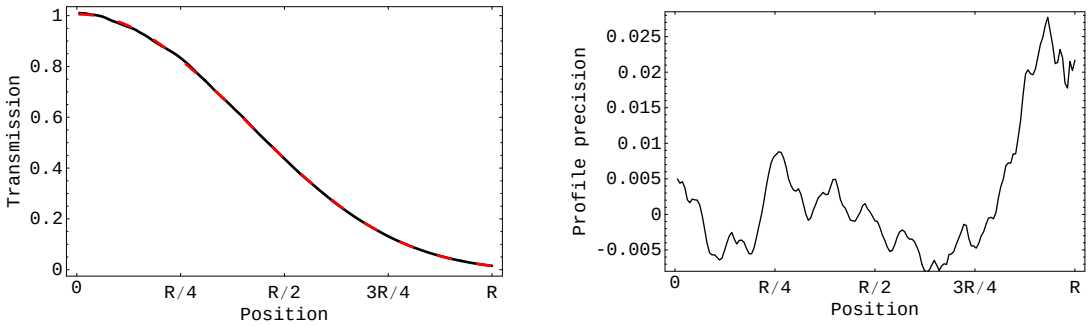

Figure 8. Same as Fig. 7, but where we adjusted the apodizer diameter to match the theoretical profile (this assumes a possible error on the apodizer diameter). The profiles match extremely well, with a maximum relative error of 2.5% at the edge of the pupil. This suggests a possible error on the apodizer diameter. We will investigate further the cause of the transmission error.

outside the aperture. This bright ringing is coming from the diffracted light of the on axis object by the FPM (Fig. 9).

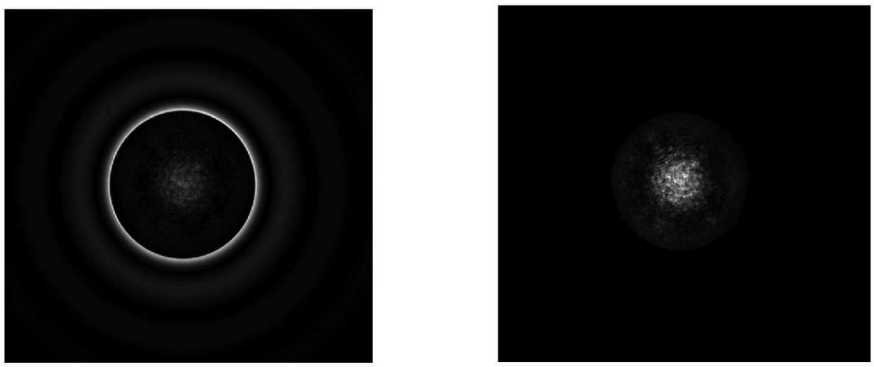

Figure 9. Left: Image of the pupil plane with the apodizer and the FPM in. The light is diffracted outside the pupil. right: Image of the pupil plane with the apodizer, the FPM and the LS in.

The Lyot Stop (LS) is placed in the pupil plane. Fig. 10-left shows the final images obtained in the focal plane. The radial average of the final farfield image is given in Fig. 10-right. The contrast obtained is better than 10^{-6} after 3 λ/d and better than 10^{-7} after 10 λ/d, which is slightly worse than expected from the simulations. The scale in λ/d is set by the system diffraction FWHM. We do have some phase aberrations in the system as

well as amplitude variations caused by phase and amplitude mixing,[15] explaining the difference. We do expect to correct some of the low order aberrations with the MEMS and improve the contrast in the 3-5 λ/d range (section 5).

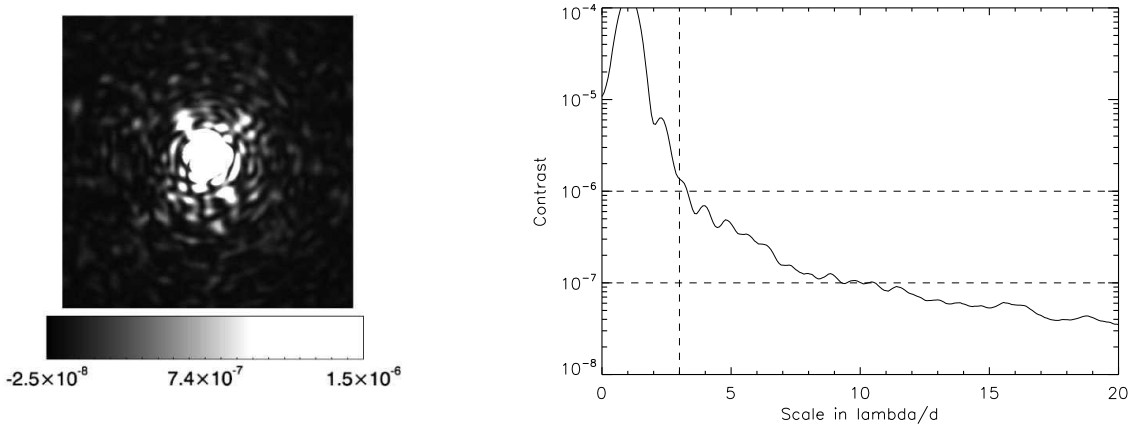

Figure 10. Contrast achieved without correcting for the static aberrations of the system. Left: farfield image. Right: Radial average of the raw contrast in the farfield image.

The rejection ratio is another way to quantify the efficiency of the coronagraph, which is the total intensity of the pupil with the three main components in (Apodizer, FPM and LS). WE found a rejection ratio of 10^{-4} in average. Overall the performance of the APLC is very promising and better than our previous tests made with the prolate shaped pupil and simple LC.

4.2 Comparison with expected performances

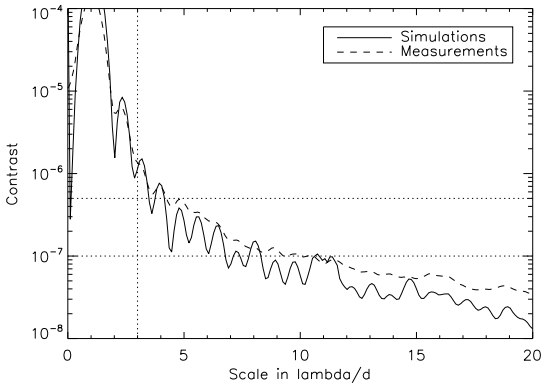

Figure 11. Comparison between simulations (full line) and measurements (dashed line).

We compared these results to a simulation of the testbed, developed using Fresnel propagations. Without loss of information we simulated a simplified version of the testbed where we removed the folding mirrors and we replaced the powered mirrors with lenses. For more details on the simulations, see Thomas el al.[15] Fig. 11 shows the comparison between results and simulations. The apodizer intensity distribution used in the simulations uses the data of Fig. 6. Therefore, it includes some of the amplitude variations from the system.[15] The simulations are only slightly better (less than a factor 2) up to 10 λ/d. The measurements then show more high power at higher frequencies.

We also performed a study of the Lyot plane intensity. If Fig. 12, we show a comparision between the Lyot plane image and a theoretical simulation of the perfect Lyot plane. The general structure is identical, but significant leakage exists inside the aperture, therefore reducing the contrast in the final image. In Fig. 13, we compare the actual image of the Lyot plane with a perfect numerical propagation using the measured apodizer as input and the corresponding theoretical mask size. Both images are very similiar which suggest that the leakage is mostly due to the apodizer profile. In Fig. 14, a simulation using the measured apodizer and a mask size 7.8% larger than the theoretical value corresponds to the minimum leakage inside the pupil.

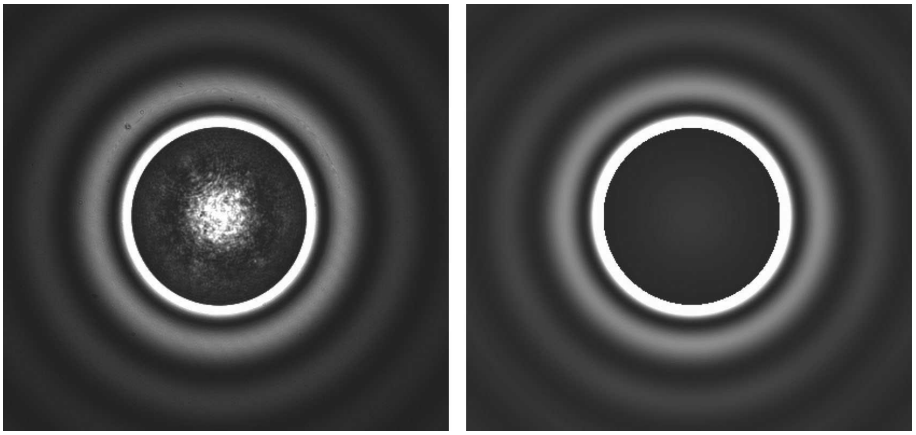

Figure 12. Image in the lyot plane (left) before without Lyot Stop, and simulation of perfect APLC (right). The structure outside the aperture is identical, but residual light is visible inside the pupil.

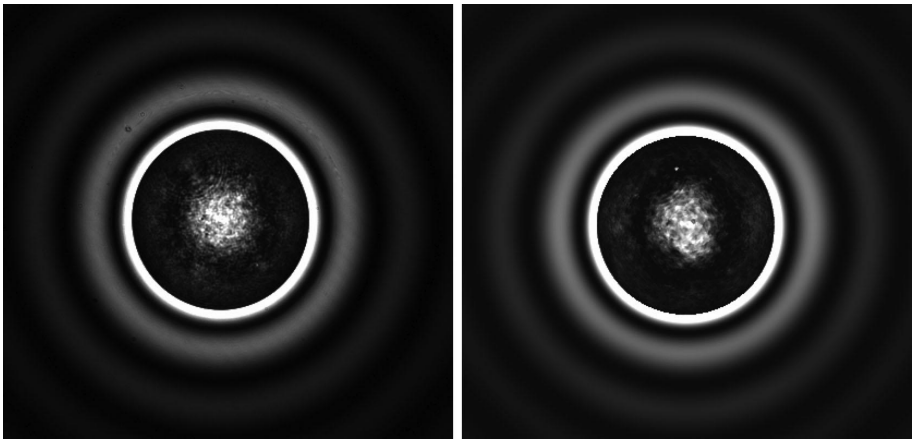

Figure 13. Comparison between the actual Lyot plane image (left) and a simulation of the Lyot plane image based on the numerical propagation of the measured apodizer and using the theoretical mask size. The main leakage inside the aperture is identical in the simulation, with a faint dark ring at about half the radius. This suggests that the main cause of the leakage is due to a mismatch in the FPM size.

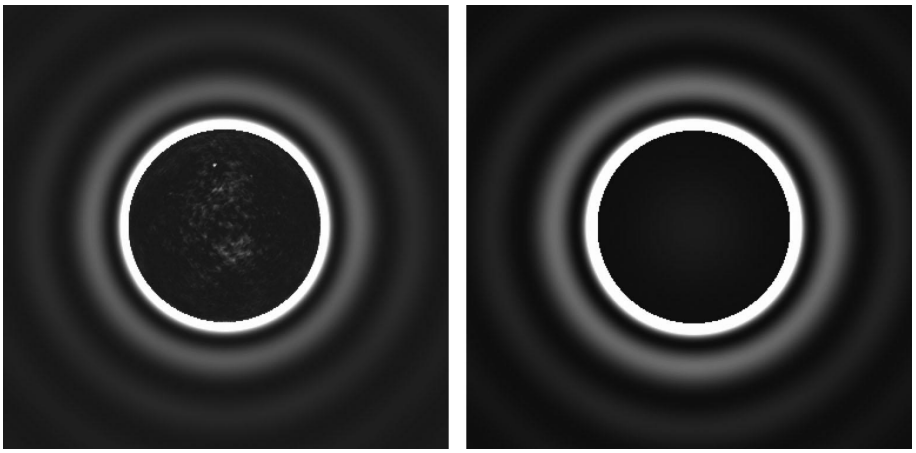

Figure 14. Comparison between the actual Lyot plane image (left) and a numerical simulation (right), based on the numerical propagation of the measured apodizer and using a mask size 7.8% larger than the theoretical FPM. This FPM size corresponds to the minimum integrated leakage inside the pupil plane.

5. TEST OF THE APLC WITH WAVEFRONT CORRECTION

The next step is to correct for the phase error of the system to try and improve the contrast. We tried two different approaches to close the loop: with or without the apodizer. Without the apodizer, we flattened the MEMS to 0.7 nm RMS correcting controllable spatial frequencies over the full pupil and 0.5 nm RMS over 75% of the pupil size. The PSDI was used as the wavefront sensor Closing the loop with the apodizer is achievable to approximatively the same level (0.44 nm RMS for 75% of the pupil and 0.66 nm RMS for the full pupil). The slight difference might be due to some focus shifts introduced by the apodizer or by non flat illumination in the pupil. However, this is beyond the scope of this paper and we will concentrate on the first method. Since the loop was closed without the apodizer, we carefully placed it at the same position as the 10 mm hard-edge pupil used to flatten the MEMS. The wavefront correction depends significantly on the position of the pupil and how well we can control the actuators. Once positioned, we repeat the same procedure as the one used with the flat mirror. Fig. 15-left gives the farfield image obtained with the best flattening. We clearly see the dark square hole up to the Nyquist frequency. We also see the remaining speckle pattern due to the residual errors in the system. The extra spots located on a square grid are due to the MEMS actuators print through and appear at twice the Nyquist frequency. The bright dot on the bottom left of the image is probably a ghost of the PSF coming from the reflexion of the light on the window of the MEMS. The radial average is given by the dashed-dotted line of

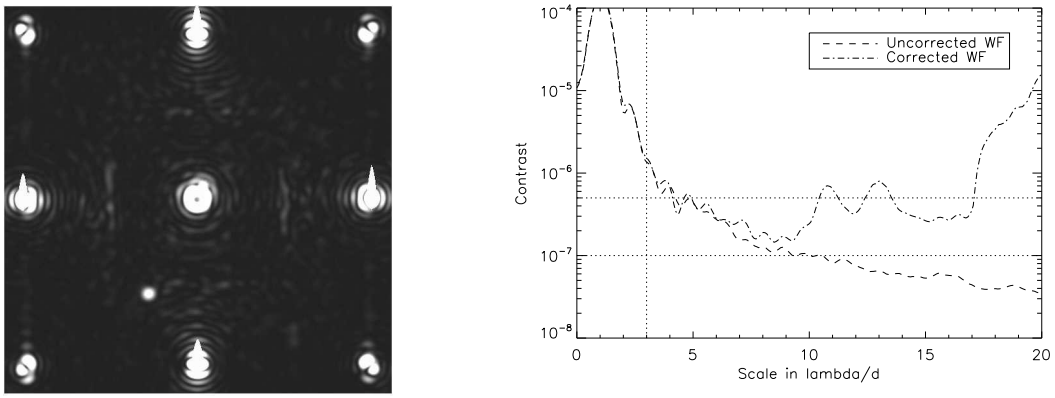

Figure 15. Contrast using the MEMS. Left: the dark zone is clearly visible and the actuator print through creates the spots at twice Nyquist frequency. Right: Radial average of the raw contrast in the farfield image.

Fig. 15-right.

The MEMS did not improve much the contrast at lower frequencies even with such a good wavefront correction and got worse after $10\lambda/d$. However, it is as good as the flat at the 3-9 λ/d which is promising. This lack of improvement might be due to non-uniform illumination, phase and amplitude mixing, or extra-aberration in the Lyot plane (between mirror M1 and M2). End to end fresnel modeling will help confirm these hypothesies.

6. ASTROMETRIC GRID

Because the intrinsic property of a coronagraph is to remove the PSF of the parent star, we need an extra reference for the astrometric and photometric calculation. The reference has to be taken at the same time as the coronagraphic image since aberrations, atmospheric seeing and other sources of errors cause the PSF to both drift and vary in intensity. Two groups[17,18] came up with the idea of placing a periodic grid of wires with known width and spacing in a pupil plane in front of the occulting coronagraphic focal plane mask to produce fiducial images of the obscured star at known locations relative to the star. We used the apodizer with the grid presented earlier to check this theory. Those tests have been made from a first batch of microdots apodizer that were affected by manufacturing errors limiting the contrast. Fig. 16 shows direct and un-occulted images of a point source for astrometry and photometry. On the direct un-occulted image, the satellite spots are barely visible. On the final occulted image however the central peak is gone and the satellites well defined.

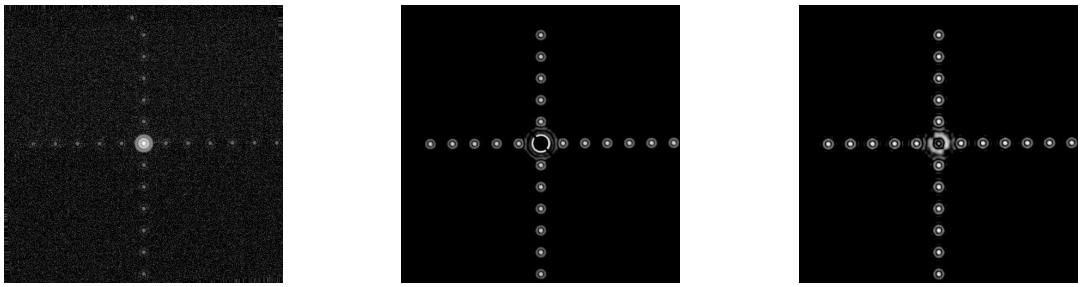

Figure 16. From left to right: direct un-occulted images, occulted image (no Lyot Stop), coronagraphic image. The intensity is normalized by the peak intensity of the un-occulted psf, the scale is logarithmic and greater than 1e-6.)

The astrometric grid turned out to also be very useful to better understand focusing and aberrations in the re-imaged pupil mode. The structure of the MEMS itself could play the same role as the diffraction grid.

7. CONCLUSION

In this paper we show the first laboratory results of our APLC at the LAO. We obtained the first coronagraphic image showing the evidence of a dark zone using a MEMS deformable mirror. We tested the contrast performance and compare it to a simulation using Fresnel propagation. We reach contrasts of 2.10^7 between 3 and 10 λ/d using a MEMS device which is close to the results obtained with a high quality gold flat mirror. We also tested the astrometric and photometric grid and confirmed that the method works with coronagraphic images.

The next steps are to study the effects of the aberrations – static and dynamic using real turbulent phase plates – on the performance of the contrast both in the simulation and with the testbed. Some preliminary tests on the stability of the PSF have been conducted by Evans et al.[7]

ACKNOWLEDGMENTS

The authors would like to gratefully acknowledge the Gordon and Betty Moore Foundation for postdoctoral support of Dr. Thomas via the Laboratory for Adaptive Optics at UC Santa Cruz. We are also grateful for AMNH Kalbfleisch research fellowship.This work was supported in part by the National Science Foundation Science and Technology Center for Adaptive Optics, managed by the University of California at Santa Cruz under cooperative agreement AST 98-76783.

REFERENCES

[1] Macintosh, B., Graham, J., Palmer, D., Doyon, R., Gavel, D., Larkin, J., Oppenheimer, B., Saddlemyer, L., Wallace, J. K., Bauman, B. , Evans, J. , Erikson, D., Morzinksi, K., Phillion, D. , Poyneer, L., Sivaramakrishnan, A., Soummer, R. , Thibault, S. and Veran, J.-P. ,"The Gemini Planet Imager", Proc. SPIE, 6272, 62720L (2006)

[2] Fusco, T., Rousset, G., Sauvage, J.-F., Petit, C., Beuzit, J.-L., Dohlen, K., Mouillet, D., Charton, J., Nicolle, M., Kasper, M. et al.," High-order adaptive optics requirements for direct detection of extrasolar planets: Application to the SPHERE instrument", Optics Express, 14, 7515-7534 (2006)

[3] Beuzit, J.-L., Feldt, M., Dohlen, K., Mouillet, D., Puget, P., Antichi, A., Baudoz, P., Boccaletti, A., Carbillet, M., Charton J. et al. "SPHERE: A Planet Finder Instrument for the VLT", In the Spirit of Bernard Lyot: The Direct Detection of Planets and Circumstellar Disks in the 21st Century, Ed Paul Kalas (2007)

[4] Belikov, R., Give'on, A., Trauger, J. T., Carr, M., Kasdin, N. J., Vanderbein, R. J. , Shi, F., Balasubramanian, K. and Kuhnert, A., "Toward 10^{10} contrast for terrestrial exoplanet detection: demonstration of wavefront correction in a shaped-pupil coronagraph", Proc. SPIE 6265, 62621A (2006)

[5] Severson, S. A., Bauman, B., Dillon, D., Evans, J., Gavel, D., Macintosh, B., Morzinski, K., Palmer, D. and Poyneer, L., "The extreme adaptive optics testbed at UCSC: current results and coronagraphic upgrade", Proc. SPIE 6272, 62722J (2006)

[6] Aime, C., Soummer, R., and Ferrari, A., "Interferometric apodization of rectangular apertures. Application to stellar coronagraphy", A&A 379, pp. 697707, (2001)

[7] Evans, J. W., Thomas, S. J., Gavel, D., Dillon, D. and Macintosh, B., "Contrast analysis and stability on the ExAO testbed", SPIE 7015, paper 7015-240 (2008)

[8] Soummer, R., Aime C., and Falloon, P.-E. , "Stellar coronagraphy with prolate apodized circular apertures", A&A 397, 1161-1172 (2003)

[9] Slepian, D. and Pollak, H. O., "Prolate spheroidal wavefunctions, Fourier analysis, and uncertainty", Bell Syst. Tech. J. 40, 43–64 (1961)

[10] Roy Frieden B., Progress in Optics 9 (1971)

[11] Slepian, D., "Prolate spheroidal wave functions", Fourier analysis, and uncertainty - IV. Extensions to many dimensions; generalized prolate spheroidal functions 43, 3009-3058 (1964)

[12] Soummer, R., "Apodized Pupil Lyot Coronagraphs for Arbitrary Telescope Apertures", 618, L161-L164 (2005)

[13] Phillion, D. and Sommargren, G., "Point Source Diffraction Interferometry with Lensless Imaging", presented at CfAO workshop on ExAO Calibration (2003)

[14] Evans, J.W., Macintosh, B. A., Poyneer, L., Morzinski, K., Severson, S., Dillon, D., Gavel, D. and Reza, L., Demonstrating sub-nm closed loop MEMS flattening, Optics Express 14, pp. 55585570 (2006)

[15] Thomas, S. J., Evans, J., Phillion, D., Gavel, D., Dillon, D. and Macintosh, B., "Amplitude variations on the ExAO testbed: Part II", SPIE 6888 in press, (2008)

[16] Aime, C., Soummer, R. and Ferrari, A., "Total coronagraphic extinction of rectangular apertures using linear prolate apodizations", A&A 389, p. 334-344 (2002)

[17] Marois, C., Lafrenire, D., Macintosh, B. and Doyon, R., "Accurate Astrometry and Photometry of Saturated and Coronagraphic Point Spread Function", ApJ 647, pp. 612-619 (2006)

[18] Sivaramakrishnan, A. and Oppenheimer, B. R., "Astrometry and Photometry with Coronagraphs", ApJ 647, pp. 620-629 (2006)